

Surfaces Decorated with Enantiomorphically Pure Polymer Nanohelices via Hierarchical Chirality Transfer across Multiple Length Scales

Divya Varadharajan, Karthik Nayani, Christoph Zippel, Eduard Spuling, Kenneth C. Cheng, Swetha Sarangarajan, Sangchul Roh, John Kim, Vanessa Trouillet, Stefan Bräse, Nicholas L. Abbott,* and Joerg Lahann*

Mesoscale chiral materials are prepared by lithographic methods, assembly of chiral building blocks, and through syntheses in the presence of polarized light. Typically, these processes result in micrometer-sized structures, require complex top-down manipulation, or rely on tedious asymmetric separation. Chemical vapor deposition (CVD) polymerization of chiral precursors into supported films of liquid crystals (LCs) are discovered to result in superhierarchical arrangements of enantiomorphically pure nanofibers. Depending on the molecular chirality of the 1-hydroxyethyl [2.2] paracyclophane precursor, extended arrays of enantiomeric nanohelices are formed from achiral nematic templates. Arrays of chiral nanohelices extend over hundreds of micrometers and consistently display enantiomeric micropatterns. The pitch of individual nanohelices depends on the enantiomeric excess and the purity of the chiral precursor, consistent with the theoretical model of a doubly twisted LC director configuration. During CVD of chiral precursors into cholesteric LC films, aspects of molecular and mesoscale asymmetry combine constructively to form regularly twisted nanohelices. Enantiomeric surfaces permit the tailoring of a wide range of functional properties, such as the asymmetric induction of weak chiral systems.

1. Introduction

Surfaces with mesoscale chirality are central to a range of emerging fields, including photonics, electronics,^[1-3] chiral recognition,^[4,5] biocompatible cell scaffolds,^[6] or asymmetric crystallization.^[7,8] Chirality, a direct consequence of mirror-image asymmetry, is one of the most fundamental structural elements in nature, enabling functions at molecular (e.g., amino acids), macromolecular (e.g., DNA), mesoscopic (e.g., collagen triple helix), and macroscopic (e.g., *Vitis vinifera*) scales. In nature, chiral precursors are assembled into macromolecular units and further into mesoscale structures, with the successive transfer of chiral information at each stage.^[9] While nature's approach to homochirality has been a source of inspiration for chemists and materials scientists, the preparation of enantiomorphically pure materials has been synthetically

D. Varadharajan, S. Sarangarajan, J. Lahann
Institut für Funktionelle Grenzflächen (IFG)
Karlsruhe Institute of Technology (KIT)
76344 Eggenstein-Leopoldshafen, Germany
E-mail: lahann@umich.edu

K. Nayani
Martin Department of Chemical Engineering
University of Arkansas
Fayetteville, AR 72701-1201, USA

C. Zippel, E. Spuling, S. Bräse
Institut für Organische Chemie Karlsruher Institut für Technologie (KIT)
76131 Karlsruhe, Germany

K. C. Cheng, J. Kim, J. Lahann
Biointerfaces Institute
University of Michigan
Ann Arbor, MI 48105, USA

K. C. Cheng, J. Kim, J. Lahann
Department of Materials Science and Engineering
University of Michigan
Ann Arbor, MI 48109-2102, USA

S. Roh, N. L. Abbott
Smith School of Chemical and Biomolecular Engineering
Cornell University
Ithaca, NY 14853, USA
E-mail: nla34@cornell.edu

V. Trouillet
Institut fuer Angewandte Materialien (IAM-ESS) and Karlsruhe Nano
Micro Facility KNMF)
76344 Eggenstein-Leopoldshafen, Germany

S. Bräse
Institute of Biological and Chemical Systems (IBCS-FMS)
Karlsruhe Institute of Technology (KIT)
76344 Eggenstein-Leopoldshafen, Germany

challenging and generally requires asymmetric separation after assembly. Helical structures are among the most widely evaluated chiral materials that have been fabricated by supramolecular self-assembly of inorganic or organic chiral building blocks^[10] as well as lithographic methods, such as direct laser writing.^[11–13] Chiral surfaces based on arrays of nanohelices up to 50 nm in diameter have been prepared using focused ion-beam deposition of metal–organic precursors. However, this technique is restricted to metals such as platinum, tungsten, and gold and is additionally limited in resolution due to the beam properties.^[14–17] Emulating nature’s multiscale chirality transfer approach, we pursued liquid crystal (LC)-templated chemical vapor deposition (CVD) polymerization of chiral precursors to fabricate enantiomorphic surfaces composed of arrays of nanohelices. Our approach builds upon recent findings that CVD of [2.2]paracyclophanes into supported LC films gives rise to extended arrays of well-defined nanofibers.^[18]

2. Results and Discussion

2.1. Formation of Chirality-Defined Superhierarchical Arrays of Nanohelices

In contrast to previous work by us and others,^[18,19] the chiral information is directly encoded in the precursor, rather than the templating LC medium, which remains achiral. We previously^[18] reported the formation of nanofibers by CVD polymerization of achiral [2.2] paracyclophane precursors into achiral and chiral nematic LC phases emphasizing the role of the template in dictating the morphology of the nanofibers. This work builds upon earlier work by our group demonstrating the use of CVD polymerization to create functional polymer coatings on a wide range of substrates.^[20–24] One of the key differences herein is our focus on the influence of the chemical nature of the precursors that allow for the fabrication of nanohelices with tunable properties. We demonstrate that templated CVD polymerization of chiral precursors results in superhierarchical arrays of nanohelices with defined chirality across multiple length scales. Consistent with this approach, CVD polymerization of two chiral precursors (S_p,S)-1-(4-[2.2]paracyclophanyl)ethanol (1S) and (S_p,R)-1-(4-[2.2]paracyclophanyl)ethanol (1R) into a nematic LC film (E7) resulted in regular arrays of nanohelices (Figure 1A). A detailed description of the preparation of the substrates as well as the CVD polymerization process has been included in the Experimental Section. Briefly, a pre-weighed amount (4 mg) of the precursor 1S or 1R was polymerized by CVD polymerization into a 10–12 μm thick nematic LC template E7 film pre-loaded into TEM grid wells placed on a homeotropically aligning glass substrate. The sublimation of the precursor was maintained at a constant rate of 0.2–0.4 \AA s^{-1} throughout the CVD polymerization process to ensure a low and uniform influx of the precursor radicals into the LC template. After complete sublimation of the precursor, the CVD polymerization was terminated, the LC phase removed and the nanohelices were harvested for further characterization. The chiral precursors 1S and 1R were prepared from the diastereomer (S_p)-4-formyl[2.2]paracyclophane using methyl lithium and further chromatographic separation, resulting in

homochiral precursors 1S and 1R (enantiomeric excess (E.E.) of >98% as described in the Supporting Information). The ^1H and ^{13}C NMR spectra (Figures S1,S2, Supporting Information) confirm the predicted chemical structure of both precursors. During templated CVD polymerization, E7 was chosen as the nematic medium,^[25] because it has a wide nematic temperature range and is highly birefringent.

After the polymerization of 1S and 1R into E7 to obtain the nanohelices as shown in Figure 1, complete removal of the templating LC phase was confirmed by internal reflection–absorption spectroscopy (IRRAS, Figure S3, Supporting Information, top) and X-ray photoelectron spectroscopy (XPS, Figure S3, Supporting Information, bottom) based on the absence of $-\text{CN}$ bands and N_{1s} signals in the respective spectra of the nanohelices. Depending on the molecular handedness of the precursor, nanohelices with exclusively counter-clockwise (CCW, 2S) or clockwise (CW, 2R) twists were observed (Figure 1B,C) as confirmed by scanning electron microscopy (SEM) analysis of an area of 250 μm^2 . In contrast, templated CVD polymerization of the achiral precursor 1A under otherwise identical conditions resulted in straight nanofibers rather than nanohelices (Figure 1D). Replacing the chiral alcohol group in 1S and 1R with alternate side groups, such as methoxyethane (PCP(CHOMeMe)), 2-methylpropan-1-ol (PCP(CHOHiPr)), or phenylmethanol (PCP(CHOHPh)) did not result in the formation of nanohelices (Figure S4, Supporting Information). This indicates that H-bonding involving the hydroxyl side group may contribute to the formation of nanohelices. Moreover, the incorporation of bulkier side groups appears to prevent the formation of nanohelices, presumably due to steric effects.

When comparing surfaces decorated with arrays of 2S and 2R with each other and to that of the achiral nanofibers composed of 2A, identical chemical compositions were observed by XPS (Figure 1E; Figure S5, Supporting Information) and IR spectroscopy (Figure S3, Supporting Information, top). The chemical compositions were also comparable to the respective polymer films prepared by CVD polymerization of 1S and 1R in the absence of a templating LC medium (Figure S6, Supporting Information). The chemical equivalence of both 2S and 2R surfaces, as well as chiral and achiral surfaces, is further corroborated by close-to-identical intensity ratios for $(\text{C}-\text{O})/[(\text{C}-\text{C},\text{C}-\text{H}) + (\pi-\pi^*)]$. After removing the support, circular dichroism (CD) spectroscopy of nanohelical dispersions of either 2S or 2R in methanol indicates mirrored signals at 242 nm of similar magnitude and opposite Cotton effects (Figure 1F, blue and green curves). The mirror image signals imply that the chirality of the chiral inducers, that is, 1S and 1R, determines the helical sense of the polymer assembly in the nanohelices. The positive and negative bisignate Cotton effects indicate right- and left-handed screw structures, respectively, according to the exciton coupling theory.^[26] Hence, 2S showing a negative bisignate Cotton effect has a left-handed π -stacked structure with M-helicity, while 2R with a positive bisignate Cotton effect features a right-handed structure with P-helicity. For comparison, the CD spectrum of disperse on of 2A did not show any discernible signals (Figure 1F, black).

All nanohelices showed a continuous increase in diameter from ≈ 50 nm at the base, corresponding to the approximate diameter of a single nanofiber to about 350 nm at the top.

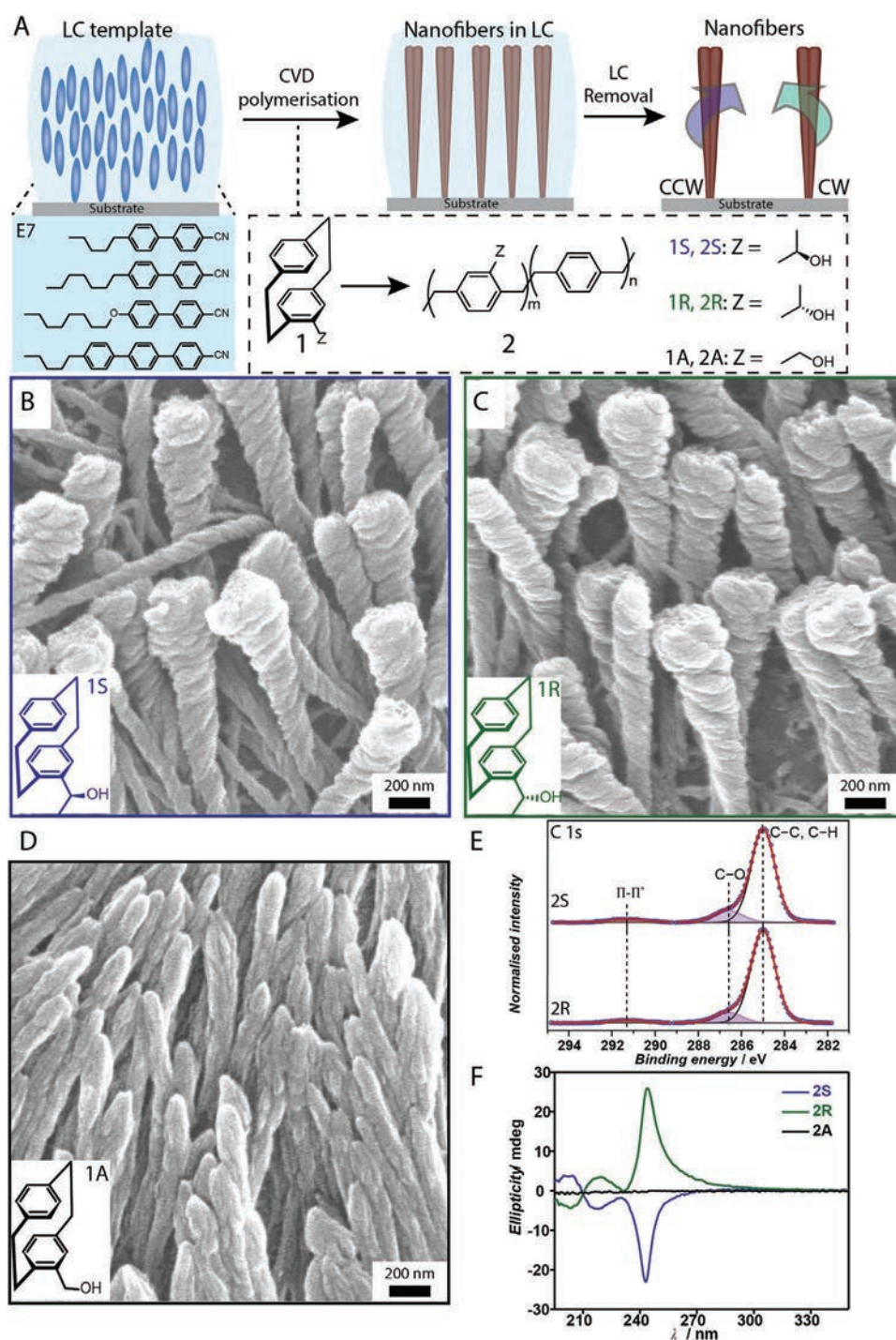


Figure 1. Templated synthesis of polymer nanohelices via CVD polymerization into a nematic LC film. A) Schematic representation of nanohelices 2S and 2R templated into the nematic E7 phase. Inset: Chemical representation of CVD polymerization of chiral and achiral precursors. B–D) SEM images of nanohelices 2S and 2R and achiral nanofibers 2A prepared by CVD polymerization of 1S (B), 1R (C), and 1A (D), respectively (the LC is homeotropically anchored on a surface before polymerization and was removed prior to SEM). E) High-resolution C1s XPS spectra of 2S and 2R confirming identical chemical composition for nanohelices with opposite handedness; these spectra are identical to the achiral nanofibers 2A shown in Figure S5, Supporting Information. See ref. [18] for a control spectrum. F) Circular dichroism (CD) spectra of nanohelices 2S (blue) and 2R (green) and achiral nanofibers 2A (black).

The average nanohelix lengths and widths (measured at full width half maxima) were $3.2 \pm 2.2 \mu\text{m}$ and $184 \pm 51 \text{ nm}$ for 2R and $2.7 \pm 1.6 \mu\text{m}$ and $188 \pm 53 \text{ nm}$ for 2S. The observed

nanohelix lengths were only about one-third of the LC film thickness (10–12 μm) and thus significantly shorter than achiral nanofibers prepared by templated CVD polymerization.^[18] We

Table 1. The contour lengths of individual nanofibers and that of the nanohelices obtained on polymerizing 1S and 1R into E7 films.

Monomer	LC film thickness [μm]	Actual length of a nanohelix [μm]	Contour length, single nanohelix [μm]
1S	10	3.22 ± 2.18	9.74 ± 4.63
1R	10	2.65 ± 1.58	8.20 ± 2.89

thus evaluated the contour length of one turn of the nanohelices, L_0 , as:

$$L_0 = \sqrt{p^2 + (2\pi R)^2} \quad (1)$$

where R is the average radius and p is the average pitch of the nanohelices. Here, the total contour length defined by a fiber in a bundle is $L_0 * n$, where n , the total number of pitch-turns for a fiber bundle (Figure S7, Supporting Information). We observed a good agreement between the LC films thicknesses used for experiments and the contour length of the fibers as presented in **Table 1**, corroborating previous findings that the thickness of the templating LC constitutes an upper limit for the length of the nanofibers.^[18]

2.2. Chirality Transfer across Multiple Length Scales

2.2.1. Role of Stereogenic Center in the Formation of Nanohelices

In principle, the chiral precursors used for templated CVD polymerization could act as chiral dopants after they enter the LC phase, thereby forming a chiral-nematic LC phase that could act as the template for the CVD polymerization. To probe this potential mechanism, the nematic LC phase was doped with either 2.28% 1S (i.e., the dimer) or 5.9% S-DMPE ((1S)-1-(2,5-dimethylphenyl)ethanol, a molecule structurally resembling the chiral monomer unit of polymer 2S). The amount of dopant used in these studies is comparable to other studies with chiral-nematic LC phases.^[27,28] However, neither 1S nor S-DMPE resulted in the formation of a chiral-nematic phase as demonstrated by the polarized light microscopy (PLM) images shown as insets in Figure S8, Supporting Information. Subsequent CVD polymerization into the 1S- and S-DMPE-doped LC phases using the achiral precursor 1A resulted in the formation of nanofibers without any discernable sign of helicity (Figure S8C,D,G,H, Supporting Information). In contrast, CVD polymerization of the chiral precursor 1S under otherwise identical conditions resulted in the formation of nanohelices (Figure S8A,B,E,F, Supporting Information). Based on these findings, we concluded that the chiral precursors used for CVD polymerization were not able to induce the formation of a chiral-nematic LC phase—ruling out direct doping by the precursor as the origin of the nanohelices. However, the presence of a stereogenic center in the CVD precursors appeared to be a prerequisite for the templated synthesis of nanohelices, suggesting a chirality transfer across the continuum of molecular, macromolecular, and microscopic scales.

For enantiomerically pure nanohelices 2S (Figure 1), the pitch varied between 108 ± 7 nm and 156 ± 10 (100% 1S).

Diluting the chiral content by templated CVD polymerization of mixtures of 1S and the achiral 1A resulted in an increased pitch and the appearance of more loosely wound nanohelices (**Figure 2A**). While the (90% 1S + 10% 1A) mixture had a p value of 160 ± 12 nm, further addition of the achiral precursor resulted in a significantly larger pitch, for example, the pitch of the (20% 1S + 80% 1A) mixture was 604 ± 48 nm. These effects are further confirmed by CD spectroscopy showing a decrease in the intensity of the bisignate signals from 100% 1S + 0% 1A to 0% 1S + 100% 1A (Figure 2C).

Similarly, the enantiomeric excess (E.E.) of the chiral precursors is a determining factor of the pitch observed in nanohelices (Figure 2B): Decreasing the E.E. of 1S from 80% to 10% increased the average p value from 191 ± 21 to 743 ± 52 nm. Accordingly, the intensity of the signal at 242 nm in the respective CD spectra (Figure S9A, Supporting Information) scaled proportionally to the E.E. of the precursor. Irrespective of the E.E. of the precursor used for templated CVD polymerization, the IRRAS spectra were indistinguishable (Figure S9B,C, Supporting Information), suggesting that the composition of the respective nanohelices was identical. To better understand the mechanism of chiral transfer that results in the formation of enantiomorphically pure nanohelices, we placed our observations into the context of a simple model that considered the nanohelices and the LC as a single phase with a doubly twisted director (n) configuration,^[29] wherein the free energy associated with the orientational gradients can be expressed in terms of the Frank free energy:^[30]

$$F = \frac{1}{2} \int dV [K_{11} (\nabla \cdot n)^2 + K_{22} ((n \cdot \nabla \times n)^2 + q_0) + K_{33} (n \times \nabla \times n)^2 - 2K_{24} \nabla \cdot (n (\nabla \cdot n) + n \times \nabla \times n)] \quad (2)$$

where K_{11} , K_{22} , K_{33} , and K_{24} are the Frank elastic constants associated with splay, twist, bend, and saddle-splay deformations, and q_0 is the twisting strength. As described previously,^[29] minimization of the free energy of this model leads to the prediction that the pitch, p , changes with the twisting strength q_0 as:

$$p = \frac{8\pi (K_{24} - K_{22})}{3q_0 K_{22}} \quad (3)$$

We characterized the twisting strength as $q_0 = x$ for (1S + 1A) mixtures, where x = mole fraction of 1S, and $q_0 = x - (1 - x) = 2x - 1$ for (1S + 1R) mixtures.^[31] By assuming commonly reported values of K_{22} (≈ 10 pN) and K_{24} ($\approx 1.2 K_{22}$) for the combined system composed of polymer nanohelices and the LC phase,^[32] we calculated the pitches to monotonically decrease with increase in q_0 . This prediction is consistent with our experimental observations (Figure 2D) and supports our conclusion that the chiral strength of the stereogenic center determines the pitch of the nanohelices.

2.2.2. Higher Order Arrangement of the Nanohelices

Next, we considered higher-order arrangements of 2S and 2R nanohelices in the form of microscopic surface arrays (**Figure 3A–F**). Dependent on their respective precursor

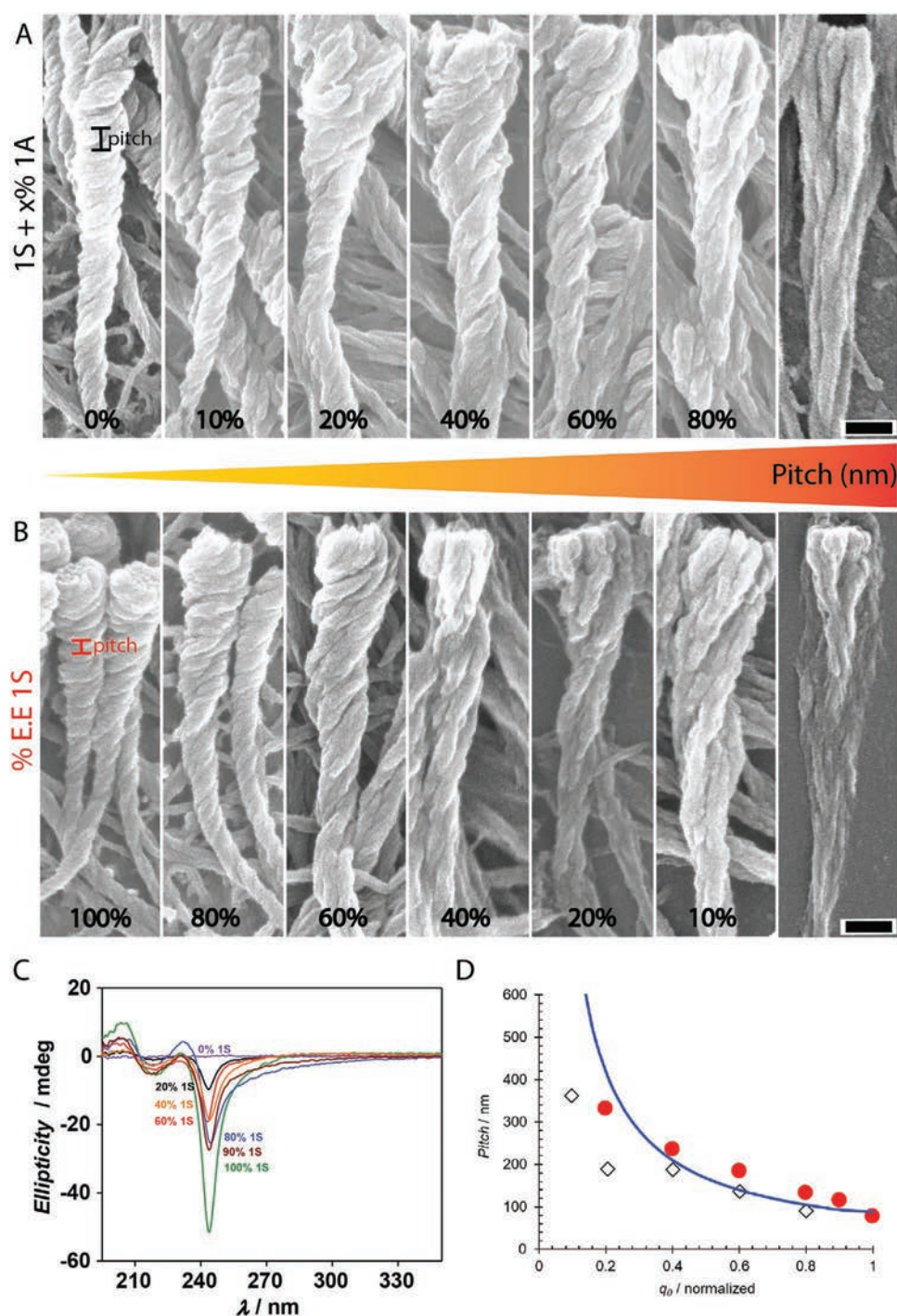


Figure 2. Enantiomeric purity of the molecular precursors defines the pitch of nanohelices during templated CVD polymerization. A) SEM images of representative polymer nanohelices prepared with varying amounts of 1S and 1A (1S + % 1A). The scale bar represents 200 nm. B) SEM images of representative nanohelices prepared with varying amounts of 1S and 1R expressed as % E.E. The scale bar represents 200 nm. C) CD spectra of the polymer nanohelices are shown in (A). D) Pitches of nanohelices from experiments (red dots) and theoretical prediction (hollow diamonds) as a function of q_0 ; the blue line represents the computed pitch.

stereochemistry, enantiomorphically pure nanohelices consistently resulted in microscopic clockwise (CW) (2R) or counterclockwise (CCW) (2S) patterns and appeared independent of the drying method. In contrast, no helical patterns are observed in arrays of achiral nanofibers (2A), evidently due to the achiral

nature of 2A. Corroborating this observation, the PLM images of nanohelices 2S and 2R after templated CVD polymerization, but prior to removal of the LC phase, also indicate the emergence of characteristic twist patterns (Figure 3C,F). While qualitatively similar, nanohelices 2S exhibited a larger twist

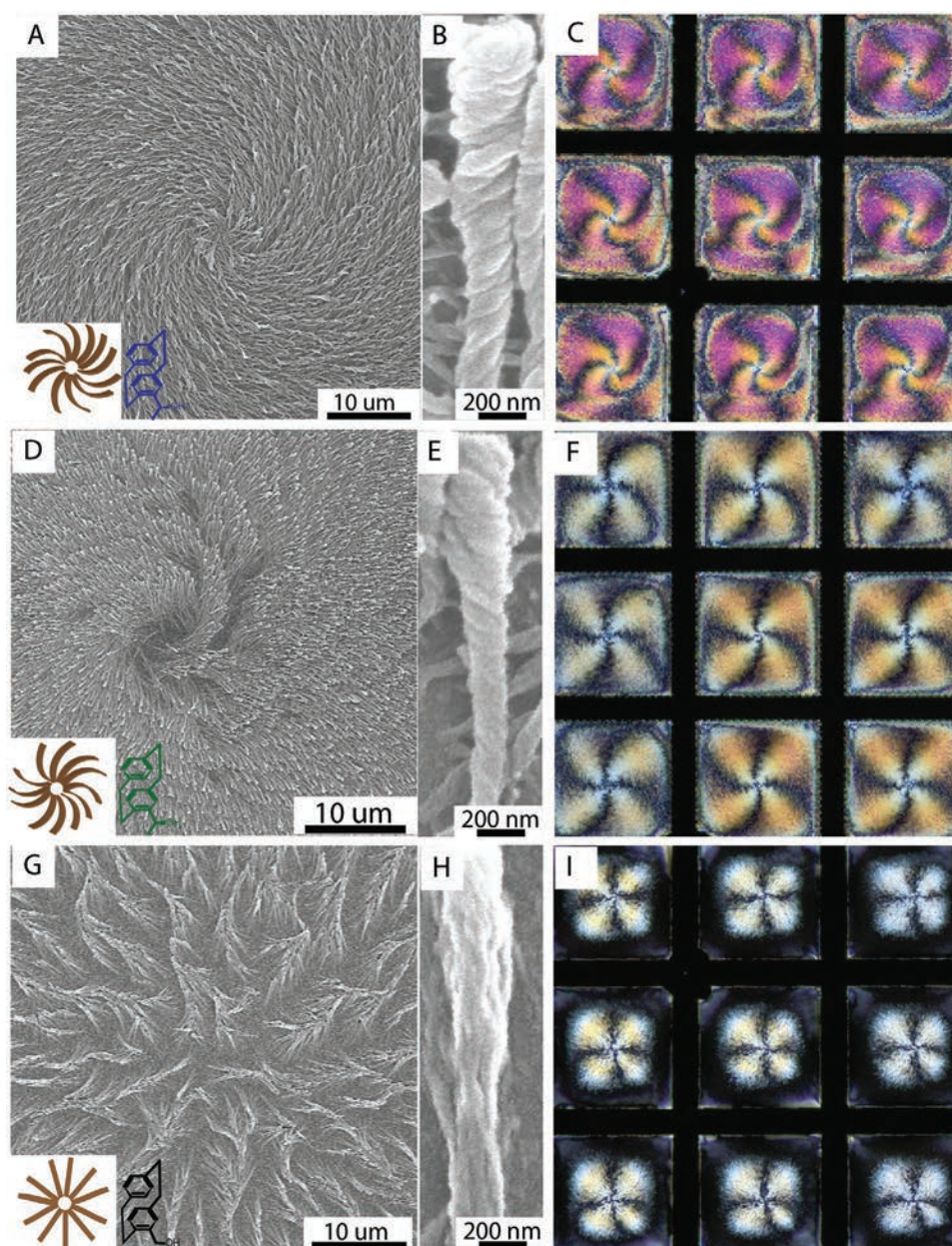


Figure 3. Large-area chirality in arrays of enantiomeric nanohelices. A–F) SEM images of nanohelices display counter-clockwise (2S, A,B) or clockwise (2R, D,E) patterns. Their corresponding POM images of LC phases after CVD polymerization are shown in (C) and (F), respectively. G,H) SEM images of polymer nanofibers prepared from 1S with a 0% E.E., and the corresponding POM image representing the LC phases after CVD polymerization is shown in (I). The insets show a schematic of the nanofiber mesoscale structures and the monomer chemical structures.

(Figure 3A–C) than nanohelices 2R (Figure 3D–F), which was attributed to differences in their respective enantiomeric purities of 99% E.E. (1S) and 97% E.E. (1R), a trend also visible in their corresponding POM images. Although a visible twist of the LC at the air interface is seen (Figure 3C,F), it does not reveal signs of the typical fingerprint textures observed in cholesteric LC phases doped with small molecules of high, twisting powers.^[33,34] This was further corroborated by the non-twisted patterns of both the nanohelices and that of the LC when a racemic precursor mixture 1S + 1R (1:1) was polymerized into the achiral E7 (Figure 3G–I).

The solid-state CD spectra of the nanohelices show broad bands at 275–339 nm and 340–700 nm both for 2S (Figure S10, Supporting Information, blue line) and 2R (Figure S10, Supporting Information, green line), but of opposite handedness due to their chiral nature. The CD spectra of the racemic precursors showed only baseline signals (Figure S10, Supporting Information, black line). As the additional broadbands are only observed for surface-supported nanohelices, but not for nanohelices after removal from the substrate, we consider these bands a cooperative property of the mesoscale assemblies that emerges from the original molecular chirality of

the precursors through superhierarchical chirality transfer, a phenomenon often observed in nature.^[35] To further elucidate this effect, nanohelices with variable E.E. from 100 to 10% 1S were prepared. For an E.E. above 80% (Figure S11, Supporting Information), superhierarchical assemblies of enantiomeric nanohelices were exquisitely controlled by the chiral purity of the precursor used for templated CVD polymerization. In contrast, we observed loss of the CCW twist for nanohelices with decreasing E.E.

2.3. Competing Chirality Effects

So far, the role of molecular chirality of the precursor during templated CVD polymerization has been the main focus of our

investigations, and thus, achiral LC phases were employed. It is however worthwhile to explore how competing chiral information from the precursor and the templating LC phase may influence the formation of nanohelices. Replacing the nematic E7 phase with a cholesteric phase resulted in nanohelices displaying composite features that can be attributed to the chiral precursor (e.g., closed-looped pitch) and the templating cholesteric phase (e.g., curved fiber shape, Figure 4).

SEM images of nanohelices obtained by templated CVD polymerization of the chiral precursors 1S and 1R into cholesteric LC phases composed of E7 and 2.4 wt% of either S- or R-811 dopants reveal nanohelices that resembled the nanohelices formed in an achiral E7 phase with regards to their tight pitches, but, additionally, displayed CW or CCW bends with a radius of curvature of $1.80 \mu\text{m}^{-1}$ (Figure 4B,C and lower

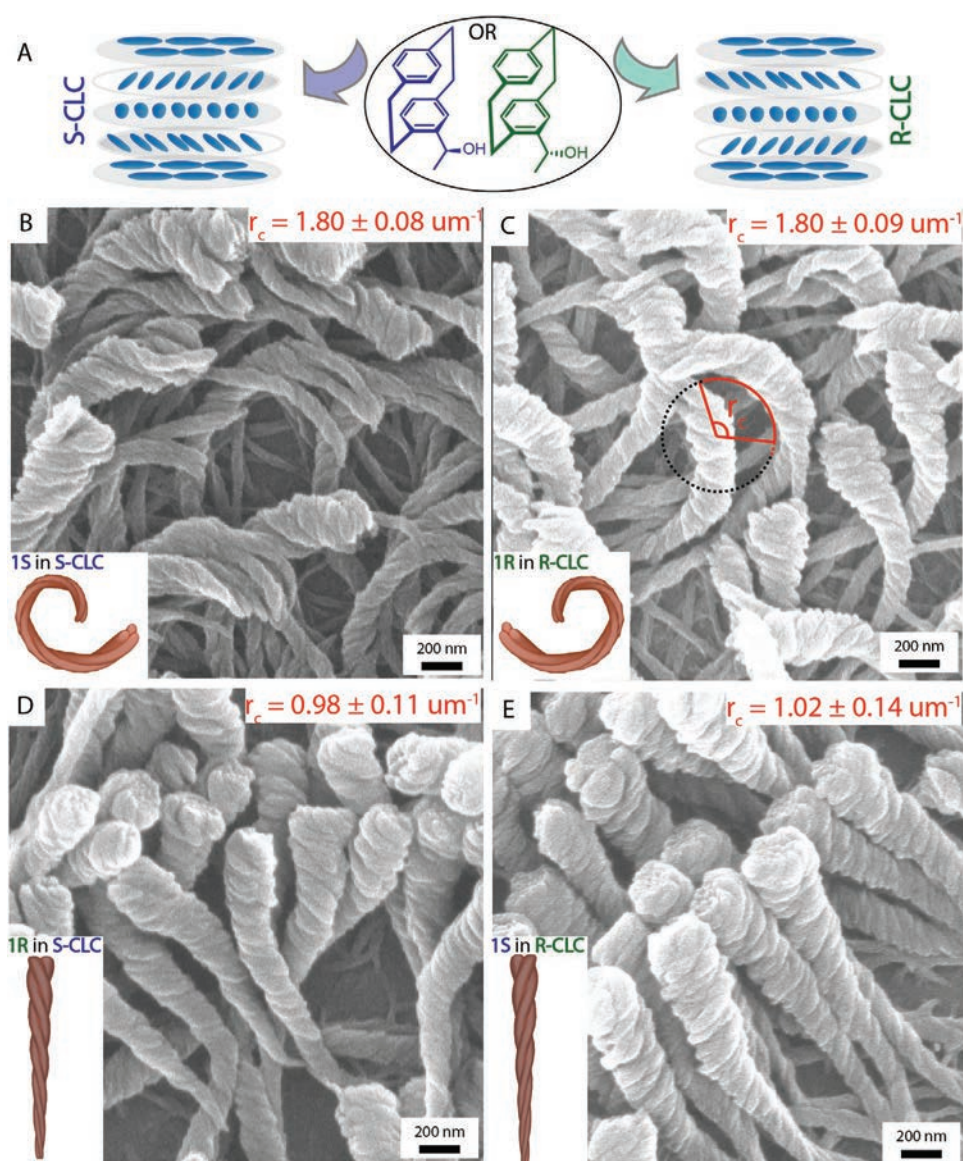


Figure 4. Templated synthesis of nanohelices using cholesteric LCs. A) Schematic representation of templated CVD polymerization of precursors 1S and 1R into S- (E7 doped with 2.4 wt% S-811) and R-configured (E7 doped with 2.3 wt% R-811) LC phases. B,D) SEM of polymer 2S (B) and 2R (D) templated by the S-CLC phase. C,E) SEM of polymer 2R (C) and 2S (E) templated by the R-CLC phase.

magnification images in Figure S12A,B, Supporting Information). In the case of the nanohelices shown in Figure 4B, the chiral information encoded in the precursor (1S) and the LC phase (S-811) appear to “synergize” structurally to give rise to pronouncedly bent nanohelices with radii of curvature consistently exceeding those observed for nanofibers prepared from achiral precursors ($E7 + 2.3\% S/R811 = 0.062 \mu\text{m}^{-1}$). Similar chiral complementarity was observed for the combination of 1R with the R-811 doped LC phase (Figure 4C). For the case of competing chiral information between the chiral precursor and the LC phase, that is, 1S polymerized into a R811-doped LC phase, the curving effect was suppressed, and relatively straight nanohelices were observed that were morphologically indistinguishable from nanohelices templated by the achiral E7 phase (Figure 4D,E and lower magnification images in Figure S12C,D, Supporting Information). A similar “antagonistic” effect was observed for the combination of 1R and the S811-doped LC phase. In principle, the relative effects of the two chiral contributors could be merely a question of stoichiometry with the chiral precursor overpowering the contributions from the doped LC phase. Thus, the amount of the chiral dopants S811 and R811 was systematically increased from 1% to 9%, and the resulting LC phases were used as the template for the CVD polymerization of 1S. In the synergistic case, bent nanohelices were observed in all cases, and the radius of curvature monotonically increased with increasing amounts of dopant (Figure S13, Supporting Information). Once the dopant concentration reached a threshold concentration of about 5%, multi-domain organizations appeared resembling typical fingerprint patterns previously observed in cholesteric LC phases (Figure S13C–E, Supporting Information). In the antagonistic case, that is, templated CVD polymerization of 1S into the R811-doped E7 phases, the nanohelices appeared straight, the pitch of the nanohelices remained unaltered, and their radii of curvature were consistently close to zero (Figure S14, Supporting Information). These findings suggest that chiral elements of the precursor and the templating LC phase combine into nanohelices that can display synergistic or antagonistic features over multiple length scales: i) If the chiral elements of precursor and LC phase match (that is, 1R and E7 + R811 or 1S and E7 + S811), we observe bent nanohelices where their nanoscale features are similar to what has been observed for the CVD polymerization into achiral nematic phases, while their microscopic structure matches that of the cholesteric phase. In the opposite case (i.e., 1S and E7 + R811), the nanohelices still maintain their original nanoscale structure, but their microscopic bending is drastically suppressed.

2.4. Detection of Weak Chirality Using Surfaces Decorated with Nanohelices

Next, we investigated the potential of surfaces decorated with nanohelices for the detection and enhancement of chirality in a nematic LC such as E7 doped with a chiral dopant S-DMPE, a system that otherwise appears to be achiral by CD spectroscopy (Figure S15, Supporting Information). When a drop of the same LC mixture E7 + 5% S-DMPE was cast on the chiral substrates decorated with 2R and 2S nanohelices,

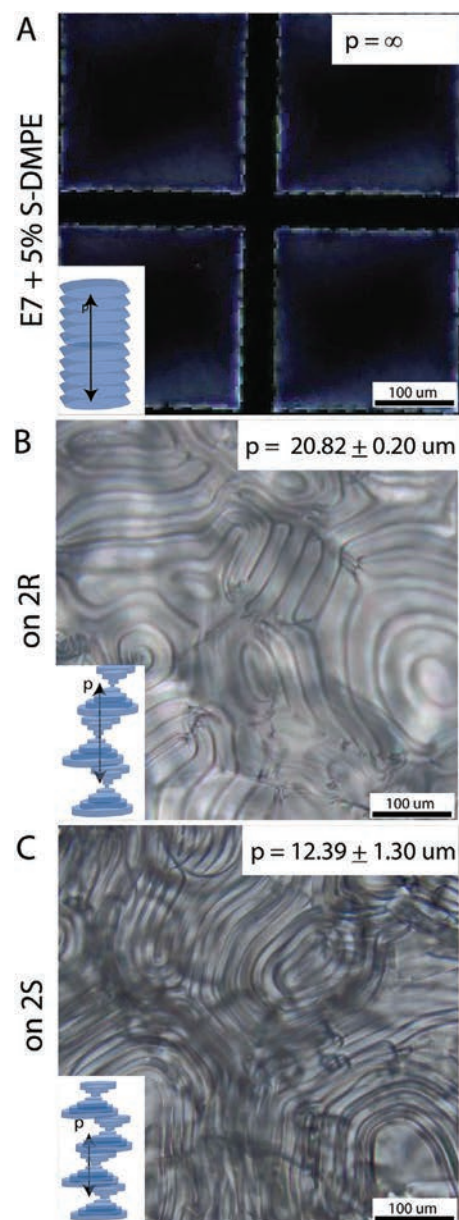


Figure 5. Chiral nanohelical assemblies as substrates for the detection of chirality in specific LC mixtures. A) E7 + S-DMPE that appears to be nematic (achiral) on a homeotropically anchored substrate and by CD spectroscopy (Figure S15, Supporting Information) shows a measurable pitch on surfaces decorated with 2R (B) and on 2S (C) nanohelices. The insets provide a schematic representation of the twist in the LC mixture, that is, their pitch on different substrates.

characteristic fingerprint textures with pitches 20.82 ± 0.20 and $12.39 \pm 1.30 \mu\text{m}$ was detected by cross-PLM (Figure 5). Two different phenomena of chiral interaction were observed: i) the pitch in the LC mixture E7 + S-DMPE was smaller with increasing amounts of the dopant concentration on both 2R and 2S nanohelical substrates (Figure S16, Supporting Information), and ii) the induced pitch was larger for the LC mixture on the chiral substrate with 2R nanohelices compared to that on 2S (Figure 5B,C). The detection of chirality was an effect of the chiral translation, and consequently, the chiral strength

of the surface-patterned nanohelices. This was proven by the absence of distinguishable fingerprint textures of LC mixtures E7 + S-DMPE when dropped on chiral 2S and 2R polymer films (Figure S17, Supporting Information).

3. Conclusions

Our results reveal that Nature's concept of multiscale chirality transfer can effectively inform the synthesis of enantiomorphic surfaces. Templated CVD polymerization of precursor molecules with a single stereogenic center resulted in enantiomorphically pure nanohelices where the E.E. defines: i) the contour length, ii) the pitch, iii) the twist angle, and iv) the mesoscale morphology of the nanohelices. Furthermore, these surface-supported nanohelices were arranged into microscopic twist patterns that displayed the homochirality encoded in the original precursor. Utilizing the transfer of chirality across length scales, such as amplifying weak chiral signatures by surfaces decorated with nanohelices shown in this work, appears to be an effective pathway toward superhierarchical chiral materials. Concomitantly, these enantiomorphically pure topologies may serve as model surfaces that will contribute to a deeper understanding of nature's way to create homochirality via multiscale chirality transfer.

4. Experimental Section

Materials: Sulfuric acid (98%, VWR), hydrogen peroxide (H₂O₂, 30%, VWR), dimethyloctadecyl[3-(trimethoxysilyl)propyl]ammonium chloride (DMOAP, VWR), E7 (Merck Japan), (1S)-1-(2,5-dimethylphenyl)ethanol (S-DMPE), and (1R)-1-(2,5-dimethylphenyl)ethanol (R-DMPE) (95%, Sigma Aldrich), (R)-2-octyl 4-[4-(hexyloxy)benzoyloxy]benzoate (R811, 97%, Sigma Aldrich), S-(+)-2-octyl 4-(4-hexyloxybenzoyloxy)benzoate (S811, 95%, Sigma Aldrich), acetone (EMSURE ACS, VWR), and ethanol (EMSURE ACS, VWR) were used as received. Menzel microscope slides (Haeberle, prewashed and polished, 76 mm × 26 mm × 1 mm) were cut into ≈1 cm × 1 cm wafers and used as substrates for the preparation of nanohelices. TEM grids (Cu grids, 75 mesh, 3.05 mm diameter, Plano) were used as purchased. Quartz glass plate (20 mm diameter, Suprasil QS, Hellma Optik, Jena, Germany) was cleaned and pre-treated prior to usage for CD spectroscopy as described in the "Circular Dichroism Spectroscopy" section. The starting materials, solvents, and reagents for the synthesis of 1S/R/A were purchased from Carbosynth ([2.2]paracyclophane, ≥99%) and Sigma Aldrich (dichloromethyl methyl ether, 98%; lithium aluminum hydride, 95%; methyl lithium, 1.6 M in Et₂O; titanium tetrachloride, ≥97%) and were used without further purification. For reactions, extractions, and chromatography, solvents of p.a. quality were purchased from Fisher Scientific or Merck. For moisture and/or air-sensitive reactions, anhydrous solvents were taken from a solvent purification system.

X-ray Photoelectron Spectroscopy: XPS measurements were performed using a K-Alpha+ XPS spectrometer (ThermoFisher Scientific, East Grinstead, UK). All samples were analyzed using a micro-focused, monochromated Al K α X-ray source (4100 μ m spot size). The kinetic energy of the electrons was measured by a 180° hemispherical energy analyzer operated in the constant analyzer energy mode (CAE) at 50 eV pass energy for elemental spectra. The K-Alpha+ charge compensation system was employed during analysis, using electrons of 8 eV energy and low-energy argon ions to prevent any localized charge build-up. For data acquisition and processing, the Thermo Advantage software was used. The spectra were fitted with one or more Voigt profiles (BE uncertainty: \pm 0.2 eV), and Scofield sensitivity factors were applied for

quantification.^[36] All spectra were referenced to the C1s peak (C–C, C–H) at 285.0 eV binding energy.

Light Microscopy: Polarized optical microscopy images were obtained using an optical microscope (Olympus BX53) fitted with an LED light source, a polarizer before the sample, and an analyzer after the sample. The polarizer and analyzer were positioned at 90° to each other to visualize the LC textures.

Scanning Electron Microscopy: SEM images were taken using a LEO 1530 Gemini scanning electron microscope (Zeiss, Germany) at the Institute of Nanotechnology (INT), KIT. Prior to taking SEM images, all samples were stuck onto conducting carbon tapes and glued to the stub using carbon glue thoroughly to create a layer of contact between the glass substrates and the carbon tape. Further, they were sputtered with ≈6 nm of gold to prevent the charging of the polymeric fibers. All SEM images were measured at an electron accelerating voltage of 10 kV at a working distance of 2.5 mm.

Infrared Reflection–Absorption Spectroscopy: Surface-vibrational data of the fibers 2S, 2R, and 2A were recorded with a Bruker VERTEX 70 FT-IR spectrometer equipped with a Polarization Modulation Accessory 50 unit (Bruker Optik GmbH, Ettlingen, Germany). The device was cooled with liquid nitrogen and equipped with an MCT detector and a horizontal reflection unit for grazing incidence (Bruker A518). A p-polarized beam at an incident angle of 80° to the surface normal was used for measurements. The spectra resolution of all recorded spectra was 4 cm⁻¹. The sample chamber was purged for a few minutes with dry nitrogen gas before and during all measurements.

IR spectra of the polymer precursors 1S, 1R, and 1A were recorded in an FT-IR Bruker IFS 88. The compounds were measured as pure substances by an ATR technique (ATR: attenuated total reflection). The position of the absorption band was given in wavenumbers $\tilde{\nu}$ in cm⁻¹. The intensities of the bands were characterized as follows: vs = very strong (0–20% T), s = strong (21–40% T), m = medium (41–60% T), w = weak (61–80% T), vw = very weak (81–100% T).

Circular Dichroism Spectroscopy: CD measurements were performed both in solution and in solid-state (oriented CD (OCD)). For the nanohelices dispersed in methanol, measurements were performed in a J-815 spectropolarimeter (JASCO, Gross-Umstadt, Germany) in quartz glass cells (Hellma, Muellheim, Germany) with a path length of 1 mm. The spectra were recorded between 195 and 350 nm. The following measurement parameters were used: data pitch (0.5 nm), scanning speed (20 nm min⁻¹), bandwidth (1 nm), and response (4 s). Three measurements were taken for every sample, and the data were averaged over these measurements, including the subtraction of a spectrum of methanol as the baseline. All spectra were recorded at 25 °C in a thermostat-controlled cell holder. The spectra were further processed with an adaptive smoothing algorithm incorporated in the JASCO analysis software.

OCD samples were prepared by growing the nanohelices 2S, 2R, and 2A on the quartz glass plate that served as a UV-transparent window in the OCD cell. The homemade setup used for the OCD measurements is described in detail by Buerck et al.^[37] The solid-state OCD measurements were then carried out in a Jasco J-810 spectropolarimeter (Jasco, Tokyo, Japan). The quartz glass plate coated with DMOAP as the alignment agent was measured as a reference for the actual nanohelices as samples. OCD spectra were recorded between 700 and 195 nm at 8 different angles with 45° increments and averaged for each rotation angle. Three scans for each measurement at a scan rate of 10 nm min⁻¹, 4 s response time, and 1 nm bandwidth were recorded and averaged at every 45° rotation. The eight successive spectra were then averaged again and subtracted from the reference sample to obtain an accurate CD spectrum of the chiral twisted nanohelices.

Nuclear Magnetic Resonance Spectroscopy: The NMR spectra were recorded on the following NMR devices as solutions at room temperature:

¹H NMR 300 MHz and ¹³C NMR 75 MHz: Bruker Advance 300, ¹H NMR 400 MHz and ¹³C NMR 101 MHz: Bruker Advance 400, Bruker Advance Neo 400, ¹H NMR 500 MHz, ¹⁹F NMR 471 MHz, and ¹³C NMR 126 MHz: Bruker Advance III HD

Chemical shifts δ are expressed in parts per million (ppm) downfield from tetramethylsilane. References for ^1H NMR and ^{13}C NMR spectra were the residual solvent peaks of chloroform (^1H : $\delta = 7.26$ ppm) and d_1 -chloroform (^{13}C : $\delta = 77.16$ ppm), which was purchased from eurisotop. All coupling constants (J) are absolute values and are given in Hertz (Hz), whereby the indices indicate the number of bonds. The description of signals includes: s = singlet, d = doublet, t = triplet, q = quartet, quin = quintet, m = multiplet, dd = doublet of doublets, and ddd = double doublet of doublets and so forth. The spectra were analyzed according to first order. The assignments of the signal structure in ^1H NMR spectra were made by the interpretation of the chemical shifts and the multiplicity and for ^{13}C NMR spectra by DEPT 135-spectra (DEPT = distortionless enhancement by polarization transfer) and are described as follows: + = primary or tertiary C-atom (positive DEPT-signal), - = secondary C-atom (negative DEPT-signal) and Cq = quaternary C-atom (no DEPT-signal) in combination with 2D NMR techniques such as correlation spectroscopy, heteronuclear single-quantum correlation spectroscopy, and heteronuclear multiple-bond correlation spectroscopy.

Mass Spectrometry: Mass spectra were measured using electron impact (EI) or fast atom bombardment (FAB) methods and recorded on a Finnigan MAT 95. For FAB measurements, 3-NBA (3 nitrobenzyl alcohol) was used as a matrix. ESI-MS (ESI: electron spray ionization) and ASAP-MS (ASAP: atmospheric pressure solids analysis probe) spectra were measured on a series Q Thermo Scientific mass spectrometer. The peaks are quoted as mass-to-charge-ratio (m/z) and the molecule peak is given as $[\text{M}]^+$ or $[\text{M} + \text{H}]^+$ (positive mode)/ $[\text{M} - \text{H}]^+$ (negative mode) and characteristic fragment peaks are given as $[\text{M} - \text{fragment}]^+$ or $[\text{fragment}]^+$. The signal intensities are given in percent relative to the intensity of the base signal (100%). For the high-resolution mass (HRMS), the following abbreviations were used: calcd = calculated data, found = measured data.

Synthetic Protocols for 1S, 1R, and 1A: (S_p)-4-Formyl[2.2]paracyclophane was prepared according to a literature procedure by Braun et al. and was obtained with an E.E. of 98% as determined by the NMR of the diastereomeric ratio of the starting material.^[38]

Preparative Work: All reactions were carried out under argon atmosphere in oven-dried glassware using standard Schlenk techniques. Liquids were transferred with plastic syringes and steel cannula, solids were added directly as powder. If not stated otherwise, the reactions were performed at room temperature. For low temperatures, flat dewars with ice/water or isopropyl alcohol/dry-ice mixture were used. The solvents were removed at 40 °C with a rotary evaporator under reduced pressure. For solvent mixtures, each solvent was measured volumetrically.

Purification: Thin-Layer Chromatography and Column Chromatography: Analytical thin-layer chromatography was carried out on Merck silica gel coated aluminum plates (silica gel 60, F_{254}), detected under UV-light at 254 nm.

For flash column chromatography, silica gel 60 (0.040 \times 0.063 mm, 230–400 mesh ASTM) from Merck was used as stationary phase, and as mobile phase, solvents of p.a. quality were used.

Synthesis of (Rac)-4-[2.2]Paracyclophanyl)methanol (1A): The compound was prepared according to a literature procedure by Delcourt et al. The spectroscopic data are in accordance with previous reports.^[39,40]

^1H NMR (300 MHz, CDCl_3 , ppm, δ): 6.61 (dd, $J = 7.9, 1.9$ Hz, 1H, H_{Ar}), 6.56–6.45 (m, 4H, H_{Ar}), 6.41–6.37 (m, 2H, H_{Ar}), 4.71 (dd, $J = 12.8, 6.0$ Hz, 1H, CH_2OH), 4.38 (dd, $J = 12.8, 5.5$ Hz, 1H, CH_2OH), 3.40 (ddd, $J = 13.0, 10.0, 2.4$ Hz, 1H, H_{PCP}), 3.19–2.96 (m, 6H, H_{PCP}), 2.87 (ddd, $J = 13.3, 10.7, 5.8$ Hz, 1H, H_{PCP}), 1.41 (t, $J = 5.9$ Hz, 1H, CH_2OH).

^{13}C NMR (126 MHz, CDCl_3 , ppm, δ): 140.3 (C_q, C_{Ar}), 139.8 (C_q, C_{Ar}), 139.6 (C_q, C_{Ar}), 139.3 (C_q, C_{Ar}), 137.5 (C_q, C_{Ar}), 135.0 (+, CH, C_{Ar}), 133.4 (+, CH, C_{Ar}), 133.3 (+, CH, C_{Ar}), 132.4 (+, CH, C_{Ar}), 132.2 (+, CH, C_{Ar}), 132.1 (+, CH, C_{Ar}), 129.1 (+, CH, C_{Ar}), 64.5 (-, CH₂, CH₂OH), 35.3 (-, CH₂), 35.1 (-, CH₂), 34.4 (-, CH₂), 32.8 (-, CH₂).

Synthesis of (S_p ,S)-1-(4-[2.2]Paracyclophanyl)ethanol (1S) and (S_p ,R)-1-(4-[2.2]Paracyclophanyl)ethanol (1R): (S_p)-4-Formyl[2.2]paracyclophane (700 mg, 2.96 mmol, 1.00 equiv.) was dissolved in dry THF (22 mL)

and cooled to -78 °C. Methyllithium (1.6 M in diethyl ether, 2.22 mL, 3.56 mmol, 1.20 equiv.) was slowly added, and the mixture was warmed to room temperature. After 16 h, ammonium chloride (sat. aq. solution, 20 mL) was added. The phases were separated, and the aqueous layer was extracted with ethyl acetate (3 \times 20 mL). The combined organic layers were dried over sodium sulfate, and the solvent was removed under reduced pressure. After flash column chromatography (silica, n-pentane/EtOAc, 10:1) the title compound was obtained as separate diastereoisomers (S_p ,S = 1S) (300 mg, 1.2 mmol, 56%) and (S_p ,R = 1R) (115 mg, 456 μmol , 22%).

Fraction 1 (S_p ,S = 1S): $R_f = 0.34$ (n-pentane/EtOAc, 4:1)

^1H NMR (500 MHz, CDCl_3 , ppm, δ): 6.66–6.60 (m, 2H, H_{Ar}), 6.52 (qd, $J = 7.8, 1.9$ Hz, 2H, H_{Ar}), 6.47 (dt, $J = 7.9, 2.4$ Hz, 2H, H_{Ar}), 6.42 (d, $J = 7.7$ Hz, 1H, H_{Ar}), 4.95 (q, $J = 6.4$ Hz, 1H, CHCH_3), 3.34 (ddd, $J = 13.7, 10.0, 2.1$ Hz, 1H, H_{PCP}), 3.18 (ddd, $J = 13.1, 10.7, 2.1$ Hz, 1H, H_{PCP}), 3.14–3.02 (m, 5H, H_{PCP}), 2.84 (ddd, $J = 13.7, 10.7, 6.2$ Hz, 1H, H_{PCP}), 1.74 (s, 1H, CHOH), 1.30 (d, $J = 6.4$ Hz, 3H, CHCH_3).

^{13}C NMR (126 MHz, CDCl_3 , ppm, δ): 144.9 (C_q, C_{Ar}), 140.5 (C_q, C_{Ar}), 139.8 (C_q, C_{Ar}), 139.5 (C_q, C_{Ar}), 135.2 (+, CH, C_{Ar}), 135.0 (C_q, C_{Ar}), 133.8 (+, CH, C_{Ar}), 133.2 (+, CH, C_{Ar}), 132.3 (+, CH, C_{Ar}), 131.7 (+, CH, C_{Ar}), 130.0 (+, CH, C_{Ar}), 128.3 (+, CH, C_{Ar}), 68.1 (+, CH, CHOH), 35.5 (-, CH₂), 35.4 (-, CH₂), 34.5 (-, CH₂), 33.3 (-, CH₂), 25.9 (+, CH₃, CHCH_3).

IR (ATR, cm^{-1}) $\tilde{\nu} = 3616$ (s), 3608 (s), 3353 (s), 3337 (s), 3007 (w), 2968 (w), 2948 (m), 2924 (s), 2887 (w), 2847 (m), 1888 (vw), 1608 (w), 1591 (w), 1499 (w), 1448 (w), 1438 (w), 1414 (m), 1371 (w), 1320 (w), 1272 (w), 1225 (w), 1180 (w), 1145 (s), 1120 (s), 1060 (vs), 1024 (m), 963 (vw), 932 (w), 905 (s), 895 (m), 853 (s), 796 (m), 734 (w), 715 (s), 653 (s), 633 (s), 625 (s), 605 (vs), 575 (s), 558 (m), 533 (m), 521 (m), 504 (vs), 489 (s), 439 (w), and 385 (w).

MS (FAB, 3-NBA, %) $m/z = 252$ (26) $[\text{M}]^+$, 235 (100) $[\text{M} - \text{OH}]^+$.

HRMS (FAB, $[\text{M}]^+$, $\text{C}_{18}\text{H}_{20}\text{O}$) calcd.: 252.1514; found: 252.1513.

Fraction 2 (S_p ,R = 1R): $R_f = 0.27$ (n-pentane/EtOAc, 4:1)

^1H NMR (500 MHz, CDCl_3 , ppm, δ): 6.56–6.47 (m, 5H, H_{Ar}), 6.39–6.34 (m, 2H, H_{Ar}), 4.87 (q, $J = 6.2, 1\text{H}$, CHCH_3), 3.66 (ddd, $J = 13.6, 10.2, 2.4$ Hz, 1H, H_{PCP}), 3.21–2.95 (m, 6H, H_{PCP}), 2.91 (ddd, $J = 13.6, 10.8, 5.8, 1\text{H}$, H_{PCP}), 1.59 (d, $J = 6.5, 3\text{H}$, CHCH_3), 1.33 (d, $J = 5.8$ Hz, 1H, CHOH).

^{13}C NMR (126 MHz, CDCl_3 , ppm, δ): 142.4 (C_q, C_{Ar}), 140.4 (C_q, C_{Ar}), 139.7 (C_q, C_{Ar}), 139.6 (C_q, C_{Ar}), 138.7 (C_q, C_{Ar}), 135.8 (+, CH, C_{Ar}), 133.5 (+, CH, C_{Ar}), 133.2 (+, CH, C_{Ar}), 132.8 (+, CH, C_{Ar}), 132.1 (+, CH, C_{Ar}), 129.9 (+, CH, C_{Ar}), 129.8 (+, CH, C_{Ar}), 67.7 (+, CH, CHOH), 35.4 (-, CH₂), 35.3 (-, CH₂), 34.9 (-, CH₂), 33.5 (-, CH₂), 21.3 (+, CH₃, CHCH_3).

IR (ATR, cm^{-1}) $\tilde{\nu} = 3618$ (w), 3322 (m), 3029 (w), 3007 (w), 2983 (w), 2968 (m), 2945 (m), 2922 (vs), 2888 (m), 2849 (m), 1884 (w), 1592 (w), 1499 (w), 1485 (w), 1443 (w), 1411 (s), 1368 (s), 1320 (w), 1303 (w), 1289 (w), 1271 (w), 1242 (w), 1224 (w), 1204 (w), 1181 (w), 1146 (m), 1120 (w), 1077 (vs), 1060 (s), 1027 (s), 955 (w), 935 (m), 901 (m), 887 (s), 850 (vs), 793 (m), 756 (m), 734 (w), 714 (vs), 681 (w), 653 (vs), 608 (vs), 567 (w), 526 (m), 504 (vs), 484 (s), 460 (w), 443 (w), 439 (w), 422 (w), 384 (w).

MS (FAB, 3-NBA, %) $m/z = 252$ (28) $[\text{M}]^+$, 235 (100) $[\text{M} - \text{OH}]^+$.

HRMS (FAB, $[\text{M}]^+$, $\text{C}_{18}\text{H}_{20}\text{O}$) calcd.: 252.1514; found: 252.1514.

Preparation of Substrates for the Growth of Nanohelices and Nanofibers: Glass wafers of ≈ 1 cm \times 1 cm were cut using a diamond cutter and washed by immersing them into a bath of piranha ($\text{H}_2\text{SO}_4:\text{H}_2\text{O}_2 = 3:1$) solution and sonicating them for 20 min. They were then individually cleaned by dipping them into milliQ water followed by ethanol. The cleaned glass substrates were then coated with DMOAP to introduce homeotropic alignment in E7. For this, the piranha-washed and cleaned substrates were sonicated in DMOAP solution (2% in water in a beaker) after immersing them into the DMOAP solution for 15 min. They were then removed and washed individually with water followed by isopropyl alcohol and acetone to obtain uniformly coated glass substrates. This was verified by the clear, non-patchy appearance of the glass wafers. A total of 2–4 TEM grids, depending on the dimensions of the substrate (typically a 1 cm \times 1 cm wafer could accommodate 4 TEM grids), with a thickness of 10–12 μm were placed on every homeotropically aligned glass substrate. Lastly, 1 μL of the LC E7 was pipetted using a 0.1–10 μL micropipette and carefully loaded onto the TEM grids until the LC formed a convex meniscus within the meshes of the grids. The meshes

of the TEM grids that act as microwells for the LC were now overloaded. To obtain a flat film of LC with a uniform thickness, a capillary tube was used to carefully remove the excess LC in every TEM grid.

In the case of cholesteric LCs, the same procedure was followed for loading them into the TEM grids and removing the LC excess to obtain an even thickness of the film, except that they were loaded in their isotropic phase. A cleaned and homeotropically aligned glass substrate covered with the TEM grids was placed on a hot plate set to 70 °C (10 °C higher than the nematic-isotropic transition temperature of the nematic LC, E7 in this case as the nematic LC doped with the chiral dopant). After 1–2 min, when the glass wafer was hot, the CLC was carefully loaded onto the TEM grids using a 0.1–10 µL micropipette without touching the TEM grids, glass wafer, or the hot plate. As soon as the CLC was loaded, it turned transparent as it was in its isotropic phase. As described earlier, a capillary tube was used to carefully remove the excess CLC while on the hot plate to obtain a uniform thickness of the CLCs on the TEM grids. At this stage, the substrates were slowly cooled down to their nematic phase by turning off the hot plate and allowing it to cool down to room temperature under ambient conditions. The glass substrates with the TEM grids loaded with nematic or cholesteric LCs were then ready for CVD polymerization. A similar procedure for cleaning, aligning the substrate, and loading the LCs into the TEM grids as described above on a glass substrate was performed on silicon, gold, and quartz substrates for XPS, IRRAS, and OCD measurements.

Growth of Nanohelices and Nanofibers by CVD Polymerization: 4 mg of the monomer 1S, 1R, or 1A was loaded into a quartz boat with a magnetic bar and placed at the far end of the CVD quartz tube from the furnace. The substrates loaded with LCs were placed in the deposition chamber where the stage was set to 15 °C (E7 exists in its nematic phase) and rotated at 30 rpm throughout the polymerization process. The furnace was set to 550 °C in the central zone of a three-zone furnace. The other two zones were set to 560 and 500 °C, and the wall temperature around the deposition to 80 °C. Once the precursor and the substrates were placed in their respective chambers, the deposition chamber and the quartz tube were closed, and the entire system was evacuated. In about 10 min, when the vacuum reached a stable pressure of ≈ 0.009 Torr, argon was flushed through the end of the quartz tube at a constant rate of 20 sccm. When the pressure again stabilized at ≈ 0.130 Torr, the monomer boat was moved toward the furnace and placed at a distance of 3 cm from it. At this distance, the monomer begins to sublime, being placed at around 120 °C. As soon as the boat containing the monomer was placed at 3 cm distance from the furnace, the deposition controller was turned on, and the deposition of the monomer onto the substrates was monitored. A constant deposition rate of 0.2–0.4 Å s⁻¹ was maintained throughout the deposition process. When the readout was zero, the monomer boat was pulled back to its starting position. The argon supply was turned off, and the entire system was brought back to atmospheric pressure to enable the removal of the substrates from the deposition chamber.

Washing the Nanohelices to Remove LC: All substrates after CVD polymerization were individually washed in acetone followed by ethanol for 3 min each. This cycle was repeated three times to ensure the complete removal of LC from the nanohelices and the substrate. During washing, the substrates were placed at 45° inside a glass vial containing the washing solvent and slowly shaken on an orbital shaker.

Drying the Substrates to Obtain Dry Nanohelices on the Substrate: After performing the washing cycles ensuring the complete removal of the LCs from the substrates, the substrates were removed from the washing solution (acetone or ethanol) and placed on a flat surface. The substrates were air-dried for 2 h to allow the residual solvents to evaporate at atmospheric pressure and room temperature. The obtained dry nanohelices on the substrates were then used for respective characterizations.

Acknowledgements

This work was in part supported by the National Science Foundation (NSF) through Grant 1916654 (J.L.) and 1916888 (N.L.A.). This work made use of the Cornell Center for Materials Research Shared Facilities which are supported through the NSF MRSEC program (DMR-1719875). Financial contributions from the German Research Foundation (formally Deutsche Forschungsgemeinschaft DFG) in the framework of SFB1176 Cooperative Research Centre “Molecular Structuring of Soft Matter” (CRC1176, C2) and the cluster “3D Matter Made To Order” funded under Germany’s Excellence Strategy 2082/1-390761711 are greatly acknowledged (all S.B.).

Conflict of Interest

The authors declare no conflict of interest.

Data Availability Statement

The data that support the findings of this study are available from the corresponding author upon reasonable request.

Keywords

chirality transfer, liquid crystals, nanohelices, paracyclophane, polymerization, templates

- [1] X. Feng, V. Marcon, W. Pisula, M. R. Hansen, J. Kirkpatrick, F. Grozema, D. Andrienko, K. Kremer, K. Müllen, *Nat. Mater.* **2009**, *8*, 421.
- [2] Y. Yan, R. Wang, X. Qiu, Z. Wei, *J. Am. Chem. Soc.* **2010**, *132*, 12006.
- [3] Y. Zhang, P. Chen, L. Jiang, W. Hu, M. Liu, *J. Am. Chem. Soc.* **2009**, *131*, 2756.
- [4] T. Tu, W. Fang, X. Bao, X. Li, K. H. Dötz, *Angew. Chem., Int. Ed.* **2011**, *50*, 6601.
- [5] W. Zou, Y. Yan, J. Fang, Y. Yang, J. Liang, K. Deng, J. Yao, Z. Wei, *J. Am. Chem. Soc.* **2014**, *136*, 578.
- [6] G.-F. Liu, D. Zhang, C.-L. Feng, *Angew. Chem., Int. Ed.* **2014**, *53*, 7789.
- [7] P. Ringler, W. Müller, H. Ringsdorf, A. Brisson, *Chem. - Eur. J.* **1997**, *3*, 620.
- [8] E. M. Wilson-Kubalek, R. E. Brown, H. Celia, R. A. Milligan, *Proc. Natl. Acad. Sci. U. S. A.* **1998**, *95*, 8040 LP.
- [9] G. M. Whitesides, M. Boncheva, *Proc. Natl. Acad. Sci. USA* **2002**, *99*, 4769 LP.
- [10] G. Huang, Y. Mei, *J. Materiomics* **2015**, *1*, 296.
- [11] J. K. Gansel, M. Thiel, M. S. Rill, M. Decker, K. Bade, V. Saile, G. von Freymann, S. Linden, M. Wegener, *Science* **2009**, *325*, 1513 LP.
- [12] M. Thiel, M. Decker, M. Deubel, M. Wegener, S. Linden, G. von Freymann, *Adv. Mater.* **2007**, *19*, 207.
- [13] Z. Yang, M. Zhao, P. Lu, *Opt. Express* **2011**, *19*, 4255.
- [14] M. Esposito, V. Tasco, M. Cuscunà, F. Todisco, A. Benedetti, I. Tarantini, M. De Giorgi, D. Sanvitto, A. Passaseo, *ACS Photonics* **2015**, *2*, 105.
- [15] M. Esposito, V. Tasco, F. Todisco, A. Benedetti, D. Sanvitto, A. Passaseo, *Adv. Opt. Mater.* **2014**, *2*, 154.

- [16] S. Matsui, in (Ed: B. Bhushan), Springer, Berlin **2010**, pp. 211–229.
- [17] I. Utke, P. Hoffmann, J. Melngailis, *J. Vac. Sci. Technol., B: Microelectron. Nanometer Struct.–Process., Meas., Phenom.* **2008**, *26*, 1197.
- [18] K. C. K. Cheng, M. A. Bedolla-Pantoja, Y.-K. Kim, J. V. Gregory, F. Xie, A. de France, C. Hussal, K. Sun, N. L. Abbott, J. Lahann, *Science* **2018**, *362*, 804 LP.
- [19] K. Akagi, G. Piao, S. Kaneko, K. Sakamaki, H. Shirakawa, M. Kyotani, *Science* **1998**, *282*, 1683 LP.
- [20] H. Nandivada, H. Y. Chen, J. Lahann, *Macromol. Rapid Commun.* **2005**, *26*, 1794.
- [21] H. Y. Chen, J. Lahann, *Adv. Mater.* **2007**, *19*, 3801.
- [22] X. Jiang, H.-Y. Chen, G. Galvan, M. Yoshida, J. Lahann, *Adv. Funct. Mater.* **2008**, *18*, 27.
- [23] F. Xie, X. Deng, D. Kratzer, K. Chang, C. Friedmann, S. Qi, L. Solorio, J. Lahann, *Angew. Chem., Int. Ed.* **2017**, *56*, 203.
- [24] M. Koenig, J. Lahann, *Beilstein J. Nanotechnol.* **2017**, *8*, 2219.
- [25] W. Ye, Z. Li, R. Yuan, P. Zhang, T. Sun, M. Cai, X. Wang, J. Zhu, Y. Sun, H. Xing, *Liq. Cryst.* **2019**, *46*, 349.
- [26] N. Berova, K. Nakanishi, R. W. Woody, *Circular Dichroism: Principles and Applications*, Wiley, New York **2000**.
- [27] J. Lu, W. Gu, J. Wei, W. Zhang, Z. Zhang, Y. Yu, N. Zhou, X. Zhu, *J. Mater. Chem. C* **2016**, *4*, 9576.
- [28] W.-R. Chen, J.-C. Hwang, *Liq. Cryst.* **2004**, *31*, 1539.
- [29] G. M. Grason, *Soft Matter* **2020**, *16*, 1102.
- [30] K. Nayani, R. Chang, J. Fu, P. W. Ellis, A. Fernandez-Nieves, J. O. Park, M. Srinivasarao, *Nat. Commun.* **2015**, *6*, 8067.
- [31] C. Peng, O. D. Lavrentovich, *Soft Matter* **2015**, *11*, 7257.
- [32] E. Páram, J. Vallamkonda, V. Koning, B. C. van Zuiden, P. W. Ellis, M. A. Bates, V. Vitelli, A. Fernandez-Nieves, *Proc. Natl. Acad. Sci. USA* **2013**, *110*, 9295 LP.
- [33] L. Wu, H. Sun, *Phys. Rev. E* **2019**, *100*, 22703.
- [34] A. Wulf, *J. Chem. Phys.* **1974**, *60*, 3994.
- [35] S. M. Morrow, A. J. Bissette, S. P. Fletcher, *Nat. Nanotechnol.* **2017**, *12*, 410.
- [36] J. H. Scofield, *J. Electron Spectrosc. Relat. Phenom.* **1976**, *8*, 129.
- [37] J. Bürck, S. Roth, P. Wadhvani, S. Afonin, N. Kanithasen, E. Strandberg, A. S. Ulrich, *Biophys. J.* **2008**, *95*, 3872.
- [38] C. Braun, S. Bräse, L. L. Schafer, *Eur. J. Org. Chem.* **2017**, *2017*, 1760.
- [39] M.-L. Delcourt, S. Felder, S. Turcaud, C. H. Pollok, C. Merten, L. Micouin, E. Benedetti, *J. Org. Chem.* **2019**, *84*, 5369.
- [40] S. Sugiyama, Y. Aoki, K. Ishii, *Tetrahedron: Asymmetry* **2006**, *17*, 2847.

Repository KITopen

Dies ist ein Postprint/begutachtetes Manuskript.

Empfohlene Zitierung:

Varadharajan, D.; Nayani, K.; Zippel, C.; Spuling, E.; Cheng, K. C.; Sarangarajan, S.; Roh, S.; Kim, J.; Trouillet, V.; Bräse, S.; Abbott, N. L.; Lahann, J.

[Surfaces Decorated with Enantiomorphically Pure Polymer Nanohelices via Hierarchical Chirality Transfer across Multiple Length Scales](#)

2022. Advanced Materials, 34

[doi: 10.554/IR/1000142667](#)

Zitierung der Originalveröffentlichung:

Varadharajan, D.; Nayani, K.; Zippel, C.; Spuling, E.; Cheng, K. C.; Sarangarajan, S.; Roh, S.; Kim, J.; Trouillet, V.; Bräse, S.; Abbott, N. L.; Lahann, J.

[Surfaces Decorated with Enantiomorphically Pure Polymer Nanohelices via Hierarchical Chirality Transfer across Multiple Length Scales](#)

2022. Advanced Materials, 34 (9), Art.-Nr.: 2108386.

[doi:10.1002/adma.202108386](#)

Lizenzinformationen: [KITopen-Lizenz](#)